

The quantum origins of skyrmions and half-skyrmions in Cu_2OSeO_3

Oleg Janson,^{1,2} Ioannis Rousochatzakis,³ Alexander A. Tsirlin,^{1,2} Marilena Belesi,³
Andrei A. Leonov,³ Ulrich K. Rößler,³ Jeroen van den Brink,^{3,4} and Helge Rosner¹

¹Max Planck Institute for Chemical Physics of Solids, Dresden, D-01087, Germany

²National Institute of Chemical Physics and Biophysics, Tallinn, EE-12618, Estonia

³Leibniz Institute for Solid State and Materials Research, IFW Dresden, D-01069, Germany

⁴Department of Physics, TU Dresden, D-01062 Dresden, Germany

The Skyrme-particle, the *skyrmion*, was introduced over half a century ago and used to construct field theories for dense nuclear matter.^{1,2} But with skyrmions being mathematical objects — special types of topological solitons — they can emerge in much broader contexts.^{3–5} Recently skyrmions were observed in helimagnets,^{6–10} forming nanoscale spin-textures that hold promise as information carriers.^{11,12} Extending over length-scales much larger than the inter-atomic spacing, these skyrmions behave as large, classical objects, yet deep inside they are of quantum origin. Penetrating into their microscopic roots requires a multi-scale approach, spanning the full quantum to classical domain. By exploiting a natural separation of exchange energy scales, we achieve this for the first time in the skyrmionic Mott insulator Cu_2OSeO_3 . Atomistic *ab initio* calculations reveal that its magnetic building blocks are strongly fluctuating Cu_4 tetrahedra. These spawn a continuum theory with a skyrmionic texture that agrees well with reported experiments. It also brings to light a decay of skyrmions into *half-skyrmions* in a specific temperature and magnetic field range. The theoretical multiscale approach explains the strong renormalization of the local moments and predicts further fingerprints of the quantum origin of magnetic skyrmions that can be observed in Cu_2OSeO_3 , like weakly dispersive high-energy excitations associated with the Cu_4 tetrahedra, a weak antiferromagnetic modulation of the primary ferrimagnetic order, and a fractionalized skyrmion phase.

Skyrmionic spin textures in magnetic materials correspond to magnetic topological solitons as depicted in Fig. 1. They were first observed in the non-centrosymmetric B20 helimagnets MnSi ,^{6,7} FeGe ,¹⁰ and $\text{Fe}_{0.5}\text{Co}_{0.5}\text{Si}$.⁸ These skyrmionic textures are encountered also in a completely different branch of physics: in the theoretical description of nuclear matter.^{1,2} In this setting the skyrmions are of course not related to magnetic degrees of freedom, but rather to particles emerging from cold hadron vector fields at densities a few times that of ordinary nuclear matter. This is the density range relevant for compact astronomical objects such as neutron stars.^{13–15} The perhaps perplexing connection between these two seemingly disparate fields of physics is borne out of the underlying mathematical structures.^{3–5,13–17} The physical phenomena in the two different settings are both governed by an emerging set of differential equations with topological solitonic solutions: the skyrmions found first by Skyrme in the 1960s.¹

In this context we investigate the formation and microscopic origin of the observed magnetic skyrmions in helimagnets (Fig. 1). These skyrmions are large objects compared to the atomic length-scale: they are about three orders of magnitude larger in size than the inter-atomic lattice spacing. Understanding the origin of these nanometer-scale skyrmions therefore requires a multi-scale approach. In the above mentioned B20 helimagnets such is however not viable because all these materials are metallic. The metallicity causes low-energy, delocalized electronic and magnetic degrees of freedom to mix so that they intrinsically involve multiple energy and spatial scales, which renders a multi-scale approach presently intractable.

This is very different in the recently discovered skyrmionic material Cu_2OSeO_3 , a large band-gap Mott insulator (Fig. 2). The band gap enforces a natural separation between electronic and magnetic energy scales. Cu_2OSeO_3 is actually the first

example of an insulating material displaying the chiral helimagnetism that is desired for skyrmion formation while sharing the non-centrosymmetric cubic space group $P2_13$ of the metallic B20 phases, but with a unit cell that is much more complex, containing 16 Cu atoms. Due to the presence of a magnetoelectric coupling^{9,18} its skyrmions can be manipulated by an electric field,¹⁹ which is in principle very energy efficient as this avoids losses due to joule heating.

A multi-scale approach to elucidate the quantum origin of the skyrmion textures in Cu_2OSeO_3 has to start from a calculation of magnetic interactions at the atomic level. In a Cu_2OSeO_3 crystal, the magnetic Cu^{2+} ions make up a 3D network of corner-sharing tetrahedra (Fig. 2, b) with two inequivalent Cu sites, Cu(1) and Cu(2) that are inside Cu(1)O_5 bipyramids and distorted Cu(2)O_4 plaquettes, respectively.^{20,21} Each tetrahedron contains Cu(1) and Cu(2) in a ratio of 1:3. The resulting net of magnetic Cu ions in Cu_2OSeO_3 thus has a structure that is rather different from the previously mentioned metallic B20 helimagnets such as MnSi , in which the magnetic Mn ions constitute instead a three dimensional corner-sharing net of triangles, commonly referred to as the *trillium* lattice. The more complex crystal structure of Cu_2OSeO_3 leads to five inequivalent superexchange coupling constants J_{ij} between neighboring $S = 1/2$ copper spins i and j and also five different Dzyaloshinskii-Moriya (DM) vectors \mathbf{D}_{ij} in the microscopic magnetic Hamiltonian

$$\mathcal{H} = \sum_{i>j} J_{ij} \mathbf{S}_i \cdot \mathbf{S}_j + \mathbf{D}_{ij} \cdot \mathbf{S}_i \times \mathbf{S}_j, \quad (1)$$

where \mathbf{S}_i denotes the Cu quantum-spin at site i . We have determined these coupling constants by means of an extended set of *ab initio* density functional based electronic structure calculations. The obtained values were cross-checked by calculating the magnetic T_C and the temperature dependence of both

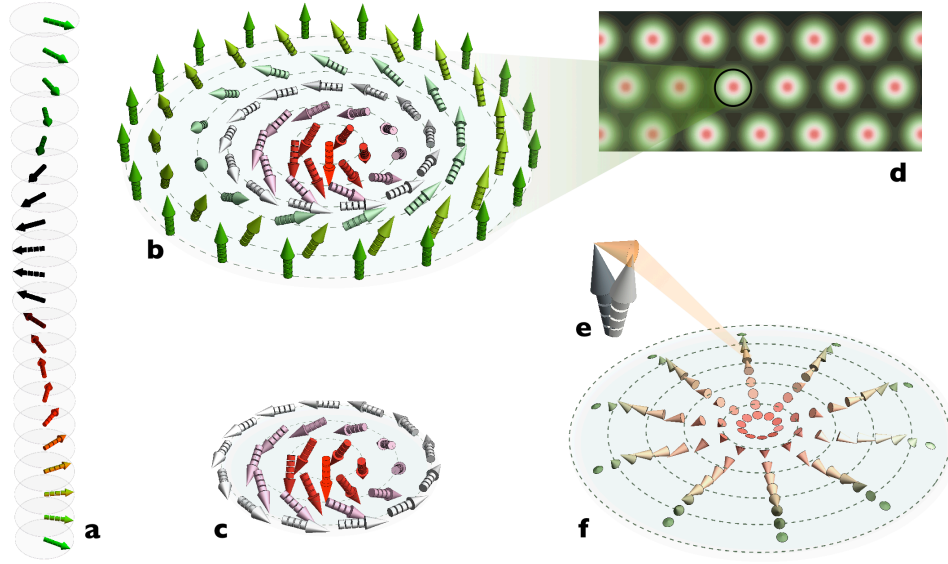


FIG. 1. Besides flat helices (a), chiral helimagnets like Cu_2OSeO_3 , manifest radially symmetric topological solitons, like skyrmions (b) or half-skyrmions (c), where the local order parameter (sectioned arrows) forms a double-twisted core, tracing out the whole (b) or half (c) of the Bloch sphere. d, Parallel skyrmions can form densely packed lattices in two spatial dimensions. e, Quantitative first-principles calculations predict that the ferrimagnetic order in Cu_2OSeO_3 is locally altered by the multi-sublattice structure. Such a canted arrangement is usually called a weak antiferromagnetic order. f, The skyrmion texture is locally composed of these three-dimensional canted spin patterns. Thus, the weak antiferromagnetic order itself is modulated along with the primary ferrimagnetic twisting shown in b.

the magnetization and magnetic susceptibility by means of large scale Quantum Monte Carlo (QMC) simulations. These simulations agreeing very well with the measurements inspire further confidence in the accuracy of the values calculated from first principles.

Having fixed the microscopic coupling constants, we proceed by establishing a hierarchy of magnetic energy scales. We first observe that the calculated J 's between Cu(1) and Cu(2) are antiferromagnetic (AFM) and between Cu(2) and Cu(2) ferromagnetic (FM). A more detailed examination of the magnetic energy scales reveals a striking difference between two groups of exchange couplings, splitting the system into two kinds of Cu_4 tetrahedra: one with strong ($|J_s| \sim 130 - 170$ K) and the other with weak ($|J_w| \sim 30 - 50$ K) superexchange couplings. The DM terms are in turn much smaller than the exchange couplings, $|\mathbf{D}_{ij}| \ll |J|$.

The four $S = 1/2$ spins of a Cu_4 tetrahedron with strong superexchange interactions can couple together to form either a total singlet, triplet or quintet state (with total spin $S_t = 0, 1$ or 2 , respectively). The tetrahedron having 3 AFM and 3 FM exchange couplings, renders the ground state (GS) a total $S_t = 1$ triplet, see Fig. 2 (b-c). The triplet GS is separated from the other spin-multiplets by a large energy gap of ~ 275 K. An important point is that the Cu_4 tetrahedron triplet wavefunction is not the classical (tensor product) state $|\uparrow\uparrow\uparrow\downarrow\rangle$ (where the double arrow labels the Cu(1) site in the tetrahedron) but rather a coherent quantum superposition of four classical states

$$|S_t = 1, M = 1\rangle = \frac{1}{\sqrt{12}} \left(3|\uparrow\uparrow\uparrow\downarrow\rangle - |\downarrow\uparrow\uparrow\uparrow\rangle - |\uparrow\downarrow\uparrow\uparrow\rangle - |\uparrow\uparrow\downarrow\uparrow\rangle \right),$$

with M labeling the three orthogonal triplet states with $M = -1, 0, 1$ (for brevity only the $M = 1$ wavefunction is given above). Although these are not the exact tetrahedron basis states due to the presence of a small triplet-quintet mixing, this representation is qualitatively correct. This effective spin wavefunction is in full agreement with the experimental observation of a locally ferrimagnetic order parameter.^{20,21} The quantum fluctuations ingrained into these triplet wavefunctions, however, give rise to a substantial reduction of the local moments, providing a natural explanation for the origin of the small moments observed experimentally.²⁰ As opposed to transversal spin fluctuations arising from spin waves (which are expected to be small in the present case owing to the dimensionality, the ferrimagnetic nature of the order parameter and the absence of frustration), these local quantum fluctuations are longitudinal in character and hence directly affect the effective magnitude of the spin. This picture is confirmed by a lattice QMC simulation for the full model of Cu $S = 1/2$ spins.

This establishes Cu_4 tetrahedra carrying magnetic triplets as building blocks in Cu_2OSeO_3 at the next step of the multi-scale approach. Within this abstraction, each of these tetrahedra can be contracted to a single lattice point. The resulting structure turns out to consist of corner-shared triangles which together constitute a trillium lattice, which is precisely the same lattice that is formed by the Mn atoms in the B20 structure of MnSi and the Fe atoms in FeGe. This establishes a very close analogy between Mott insulating Cu_2OSeO_3 and these well-known metallic helimagnets, despite the fundamental differences in electronic structure.

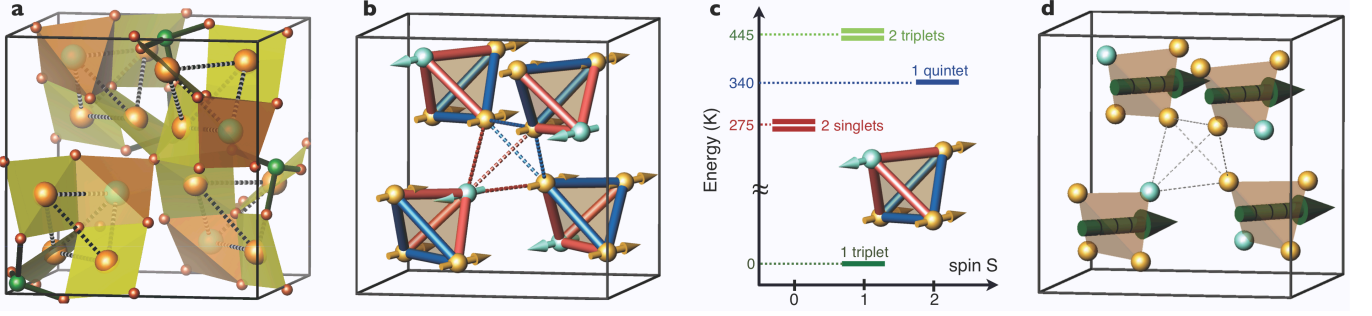


FIG. 2. Multiscale modeling of Cu_2OSeO_3 . **a**, The crystal structure is shaped by $\text{Cu}(1)\text{O}_4$ plaquettes (yellow) and $\text{Cu}(2)\text{O}_5$ bipyramids (orange), and covalent Se–O bonds (thick lines), forming a sparse three-dimensional lattice. This lattice can be tiled into tetrahedra (dashed lines), each composed of one $\text{Cu}(1)$ and three $\text{Cu}(2)$ polyhedra. **b**, The magnetic Cu^{2+} ions form a distorted pyrochlore lattice, a network of corner-shared tetrahedra. DFT calculations evidence the presence of both types of magnetic interactions — antiferromagnetic (red) and ferromagnetic (blue), in agreement with experimental magnetic structure (arrows). The strength of a certain coupling is indicated by the thickness of the respective line. The strongest couplings are found within the tetrahedra (shaded), while the couplings between the tetrahedra (dashed lines) are substantially weaker. **c**, A quantum mechanical treatment of a single tetrahedron yields a magnetic spin $S = 1$ ground state, separated from the lowest lying excitation by ~ 275 K. Due to this large energy scale, the tetrahedra behave as rigid $S_t = 1$ entities at low temperatures. **d**, The effective $S_t = 1$ entities reside at the vertices of a *trillium* lattice, exactly like the Mn ions in MnSi. Their mutual effective exchange couplings are all ferromagnetic (see text). The quantum-mechanical nature of the effective $S_t = 1$ moments is indicated by sectioned arrows.

However in Cu_2OSeO_3 , the effective triplet interactions can be derived relying on rigorous microscopic results. At this point both the weaker superexchange couplings J_w and the DM interaction D_{ij} become crucial. A straightforward perturbative calculation reveals that their net effect is a weak FM interaction between nearest-neighbor (NN) and next-nearest-neighbor (NNN) $S_t = 1$ spins, with an effective exchange coupling of about -8 K, which reflects the tendency of the system towards FM ordering. This drastic reduction of the energy scale in the effective model is caused by the renormalization of the local spin lengths and the strong quantum correlations inside the strongly coupled tetrahedra. Not only an exchange interaction, but also a DM coupling between NN and NNN $S_t = 1$ spins emerges. This is crucial because in the GS of a single strong tetrahedron all diagonal matrix elements of the DM couplings *within* the tetrahedron vanish by symmetry. The twisting mechanism that causes chiral helimagnetism in Cu_2OSeO_3 , therefore originates from the effective DM couplings *between* the strong Cu_4 tetrahedra: these will be the root cause for skyrmions to emerge.

Having established the effective trillium lattice model of Cu_2OSeO_3 , we now proceed to the long wavelength magnetic continuum theory that governs the skyrmion formation in Cu_2OSeO_3 on the mesoscopic scale. The resulting continuum equations involve two magnetic constants, \mathcal{J} and \mathcal{D} , which from a direct calculation are evaluated to be $\mathcal{J} \simeq 15$ K and $\mathcal{D} \simeq 3$ K. With the characteristic period Λ of the double-twisted skyrmion structures being $2\pi/Q$, with wavenumber $Q = \frac{\mathcal{D}}{2\mathcal{J}} \frac{1}{a}$ and lattice constant a , the calculated magnetic constants result in a helix period of $\Lambda \simeq 20$ nm which has the correct order of magnitude compared with the experimentally measured value⁹ of 50 nm. Besides this agreement with basic experimental observations, our multi-scale description also provides two essential predictions. Firstly, a very distinct set of weakly dispersive, high-energy intra-tetrahedra ex-

citation modes should appear. Secondly, a specific antiferromagnetic superstructure emerges that is the dual counterpart of the weak *ferromagnetism* present in chiral acentric bipartite antiferromagnets.²² Both these effects can immediately be tested experimentally, for instance by neutron scattering.

Having quantified in detail the microscopic couplings responsible for the chirally twisted spin order in Cu_2OSeO_3 , its magnetic phase diagram can be assessed. In the continuum description of Cu_2OSeO_3 , the Dzyaloshinskii model of chiral cubic ferromagnets, we can merge the *ab initio* parameters and the exchange stiffness \mathcal{A} (obtained from QMC calculations) to determine quantitatively the thermodynamic (Landau) potential. The value of the weakest primary coupling, the DM interaction, is fixed by the experimentally observed helix period. With this approach both the magnetic field and temperature scale are fully determined.

In this framework, one can calculate the critical field H_{c2} for the continuous transition from the conical helix state into the field-enforced ferrimagnetic collinear state. We find 80 mT at 50 K, in very good agreement with experimental data. We also determined the temperature window for the *precursor region* at around the magnetic ordering temperature where meso-phases, that are potentially of skyrmionic character, can be formed and find $\Delta T \simeq 1$ K. In this temperature interval, the skyrmionic cores are energetically favorable compared to one-dimensional helix solutions.⁵ The computed range is in agreement with the interval of about 2 K in which the so-called A-phases appear under magnetic field in Cu_2OSeO_3 crystals.^{23,24} From symmetry considerations it is immediately clear that the dominant anisotropy in Cu_2OSeO_3 is cubic with a coefficient $K_{c1} > 0$, which can stem from the magnetoelectric effect and the dielectric polarizability of Cu_2OSeO_3 . The experimental value for the magnetic field at which the conical helix closes and becomes a field-enforced saturated state fixes this anisotropy

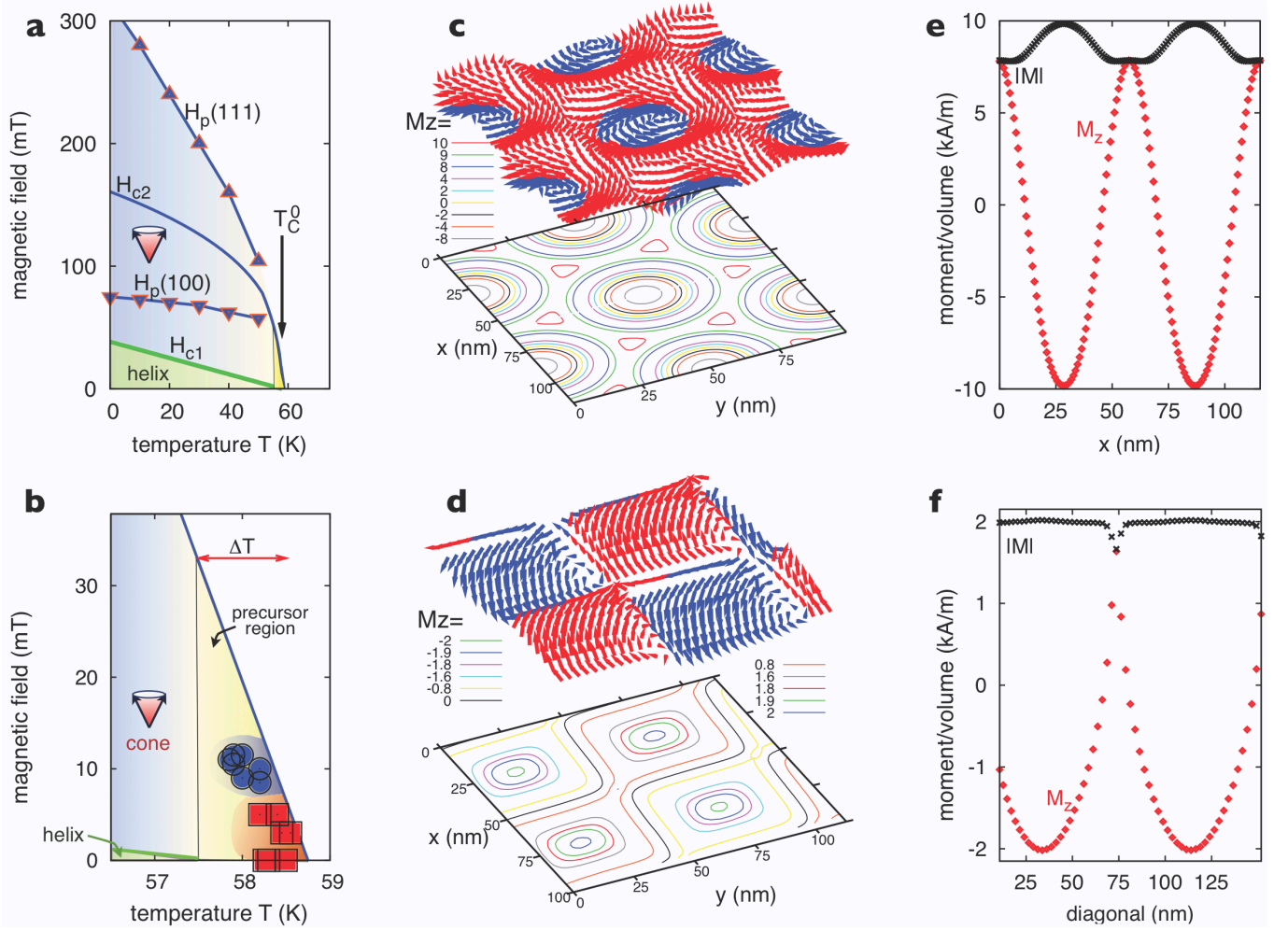


FIG. 3. Phase diagram of Cu_2OSeO_3 from Landau-Ginzburg continuum description. **a**, H_{c1} denotes the reorientation transition of the helices into the conical state. Without additional anisotropies, the cone angle closes continuously at H_{c2} and the system reaches the ferrimagnetic plateau phase. A cubic anisotropy makes H_{c2} direction depending. $H_p(111)$ denotes the continuous transition for fields along $[111]$. For fields along $[100]$ direction, the conical helix collapses by a first-order process at $H_p(100)$. **b**, The high-temperature phase diagram has a narrow precursor region where skyrmionic phases are found numerically for two-dimensional models. Blue circles show the region of stable densely packed $-\pi$ -skyrmion lattices (sketched in **c** with contour plot for component M_z and corresponding profiles across nearest neighbour skyrmions **e**); red squares mark the region of stable $\pm\pi/2$ -skyrmion lattices (sketched in **d** with profiles along a next-nearest-neighbour diagonal **f**).

at $K_{c1} M_{\text{sat}}^4 = 1.2 \cdot 10^4 \text{ J/m}^3$ (corresponding to $3.3 \mu\text{eV/Cu atom}$).

With all this in place, we can fully determine the equilibrium solutions and thereby the phase diagram (Fig. 3 a and b). In the precursor region, we find as equilibrium states two competing skyrmionic phases (Fig. 3 c to f). The first one (Fig. 3 c and e) is the standard field-driven “ $-\pi$ ”-skyrmion phase of Fig. 1(b) with the radial skyrmions ordered in a hexagonal lattice.^{3,4} The other one (Fig. 3 d and f) is the “ $\pi/2$ ”-skyrmion^{4,25} state of Fig. 1(c), which actually is the stable state at zero and low fields, because the fractionalization of skyrmions into half-skyrmions yields a higher packing density of the energetically advantageous skyrmionic cores. The fractionalized skyrmion textures contain defects like hedgehogs, narrow line or wall defects, where the magnetic order

parameter passes through zero, leading to a broad distribution of local moments that can be discernible by local probes such as μSR and NMR, or neutron diffraction methods. The emergence of the half-skyrmion phase in the vicinity of the π -skyrmion lattice of Cu_2OSeO_3 opens a new venue to study properties of textures with split topological units in experiment. Observations of these defect-ridden topological phases, together with the predicted weakly antiferromagnetic indentations of the ferrimagnetic order, the strong fluctuations of the local moments, and the weakly dispersive high-energy magnetic excitations, that are associated with the rigidly coupled spins of tetrahedra, allow to probe the quantum origin of the magnetic skyrmions in experiments on Cu_2OSeO_3 .

Acknowledgments

We acknowledge fruitful discussions with J.-P. Ansermet, A. N. Bogdanov, V. A. Chizhikov, V. E. Dmitrienko, and Y.

Onose. IR was supported by the Deutsche Forschungsgemeinschaft (DFG) under the Emmy-Noether program. OJ and AT were partly supported by the Mobilitas program of the ESF, grant numbers MJD447 and MTT77, respectively.

-
- ¹ T. Skyrme, *Nucl. Phys.* **31**, 556 (1962).
 - ² E. Witten, *Nucl. Phys. B* **223**, 422 (1983).
 - ³ A. N. Bogdanov and D. A. Yablonskii, *Zh. Eksp. Teor. Fiz.* **95**, 178 (1989).
 - ⁴ A. Bogdanov and A. Hubert, *J. Magn. Magn. Mater.* **138**, 255 (1994).
 - ⁵ U. K. Röbller, A. N. Bogdanov, and C. Pfleiderer, *Nature* **442**, 797 (2006).
 - ⁶ S. Mühlbauer, B. Binz, F. Jonietz, C. Pfleiderer, A. Rosch, A. Neubauer, R. Georgii, and P. Böni, *Science* **323**, 915 (2009).
 - ⁷ A. Tonomura, X. Yu, K. Yanagisawa, T. Matsuda, Y. Onose, N. Kanazawa, H. S. Park, and Y. Tokura, *Nano Letters* **12**, 1673 (2012).
 - ⁸ X. Z. Yu, Y. Onose, N. Kanazawa, J. H. Park, J. H. Han, Y. Matsui, N. Nagaosa, and Y. Tokura, *Nature* **465**, 901 (2010).
 - ⁹ S. Seki, X. Z. Yu, S. Ishiwata, and Y. Tokura, *Science* **336**, 198 (2012).
 - ¹⁰ X. Yu, N. Kanazawa, W. Zhang, T. Nagai, T. Hara, K. Kimoto, Y. Matsui, Y. Onose, and Y. Tokura, *Nature Commun.* **3**, 988 (2012).
 - ¹¹ F. Jonietz, S. Mühlbauer, C. Pfleiderer, A. Neubauer, W. Münzer, A. Bauer, T. Adams, R. Georgii, P. Böni, R. A. Duine, K. Evereschor, M. Garst, A. Rosch, *Science* **330**, 1648–1651 (2010).
 - ¹² A. Fert, V. Cros, and J. Sampaio, *Nature Nanotech.* **8**, 152–156 (2013).
 - ¹³ R. Ouyed and M. Butler, *Astrophys. J.* **522**, 453 (1999).
 - ¹⁴ H. Luckock and I. Moss, *Phys. Lett. B* **176**, 341 (1986).
 - ¹⁵ Brown, G. E. & Rho, M. (eds.) *The Multifaceted Skyrmion*, Chap. 6 (World Scientific, 2010).
 - ¹⁶ L. Castillejo, P. Jones, A. Jackson, J. Verbaarschot, and A. Jackson, *Nucl. Phys.* **A501**, 801 (1989).
 - ¹⁷ M. Kugler and S. Shtrikman, *Phys. Rev.* **D40**, 3421 (1989).
 - ¹⁸ M. Belesi, I. Rouschatzakis, M. Abid, U. K. Röbller, H. Berger, and J.-Ph. Ansermet, *Phys. Rev. B* **85**, 224413 (2012).
 - ¹⁹ J. S. White, I. Levatic, A. A. Omrani, N. Egetenmeyer, K. Prsa, I. Zivkovic, J. L. Gavilano, J. Kohlbrecher, M. Bartkowiak, H. Berger, and H. M. Ronnow, *J. Phys.: Condens. Matter* **24**, 432201 (2012).
 - ²⁰ J.-W. G. Bos, C. V. Colin, and T. T. M. Palstra, *Phys. Rev. B* **78**, 094416 (2008).
 - ²¹ M. Belesi, I. Rouschatzakis, H. C. Wu, H. Berger, I. V. Shvets, F. Mila, and J. P. Ansermet, *Phys. Rev. B* **82**, 094422 (2010).
 - ²² A. N. Bogdanov, U. K. Röbller, M. Wolf, and K.-H. Müller, *Phys. Rev. B* **66**, 214410 (2002).
 - ²³ S. Seki, J.-H. Kim, D. S. Inosov, R. Georgii, B. Keimer, S. Ishiwata, and Y. Tokura, *Phys. Rev. B* **85**, 220406 (2012).
 - ²⁴ T. Adams, A. Chacon, M. Wagner, A. Bauer, G. Brandl, B. Pedersen, H. Berger, P. Lemmens, and C. Pfleiderer, *Phys. Rev. Lett.* **108**, 237204 (2012).
 - ²⁵ H. Wilhelm, M. Baenitz, M. Schmidt, C. Naylor, R. Lortz, U. K. Röbller, A. A. Leonov, A. N. Bogdanov, *J. Phys.: Condens. Matter* **24**, 294204 (2012).